DOE/ER/45337-5

DOE/ER/45337--5

DE93 003654

A Progress Report
on

Fundamental Studies of Stress Distributions and Stress Relaxation in Oxide Scales on High Temperature Alloys

DE-FG02-88ER45337

submitted to
U.S. Department of Energy
Office of Basic Energy Science

by
David A. Shores
James H. Stout
William W. Gerberich

University of Minnesota
Corrosion Research Center
221 Church St.
Minneapolis, MN 55455

June 1992

TABLE OF CONTENTS

Fundamental Studies of Stress Distributions and Stress Relaxation in Oxide Scales on High Temperature Alloys

EXECUTIVE SUMMARY

Progress in the energy conversion and energy producing technologies is becoming increasingly dependent on the development of alloys resistant to high temperature oxidation. Stresses, which develop in the oxide and underlying metal as an inherent part of the oxidation process, can cause fracture or spallation of the oxide exposing the underlying alloy to renewed oxidation. If a fundamental understanding of the origin and evolution of these stresses were available, future alloy development efforts could take those factors into account to produce alloys with better oxidation resistance. This program is aimed at developing an understanding of the origin and evolution of oxidation-induced strains through a combination of experimental measurements and theoretical modeling studies.

The high temperature X-ray diffraction system developed for this program is being successfully employed to make *in-situ* measurements of the strains which develop during oxidation. This is being applied to the simple model systems, Ni/NiO and Cr/Cr_2O_3, and we have begun to isolate and identify factors which control the growth stress and thermal stress components. Our work suggests that the oxide and metal crystalline texture, the anisotropic elastic modulus and anisotropic thermal expansion can have a pronounced effect on strain state of these systems, factors which heretofore have received little attention in the literature.

Acoustic emission is being used to characterize the mechanisms of oxide scale failure (fracture) during oxidation. AE data from experiments using 304 stainless steel as a model alloy are being used to develop a statistical model of the fracture process. The strength of the metal/scale interface is an important fundamental design property that has been difficult to quantify. Using Nano-indentation and scratch techniques developed for characterizing thin film interfaces, an effort has begun to measure the fracture toughness of the metal/scale interface.

Mathematical modelling of the origin and time evolution of growth stresses is an extension and improvement of previous models developed under this contract. The current effort employs a more sophisticated stress analysis and expands the scope to include other stress relaxation processes. The interaction between the modeling studies and the X-ray diffraction measurements provides a natural credibility check to both efforts.

INTRODUCTION

The integrity of a metallic component in a high temperature oxidizing environment is dependent on the formation of a protective oxide scale. Growth stresses generated by the oxidation process, and thermal stresses arising from interfacial strains induced by thermal expansion mismatch during temperature excursions can compromise the protective capacity of a scale. These stresses can cause scale fracture, buckling or detachment of the oxide thereby exposing the underlying metal to renewed oxidation. Future alloy development will require a comprehensive understanding of both growth and thermal stresses to insure the protective capacity of oxide scales during service.

The majority of stress measurements made on metal/oxide systems have been made at room temperature, measuring the residual stress state of the system. Residual strains, however, are a complex superposition of the thermal strains that develop upon cooling, and growth strains that develop at elevated temperature as the oxide grows. The contribution which each makes to the stress state of the system can be understood only by independent measurement of the growth and thermal stress components. Residual stress measurements provide a very limited view (and in some cases, an ambiguous view) of the stresses which develop during the oxidation process. Over the course of this contract we have developed a new experimental system for measuring strain *in-situ* during oxidation, and in the present phase we are applying this equipment to measure both the growth strains and the residual strains in simple model systems such as Ni/NiO and Cr/Cr_2O_3. This report is divided into four sections which describe (I) experimental measurements of strains in oxidized metals by X-ray diffraction, (II) experimental measurements of scale fracture by acoustic emission, (III) modeling of growth stresses and (IV) experimental measurement of metal/oxide adhesion by nano-indentation and scratching techniques.

I. EXPERIMENTAL MEASUREMENTS OF STRAIN BY X-RAY DIFFRACTION

Background

The existence of stresses is easy to demonstrate, but an evaluation of their origin and magnitude is a more difficult task. Typical average values of measured residual stresses in attached oxides of up to several microns thick are on the order of a few hundred MPa in compression, (Pivin, Morvan et al., 1983; Aubry, F. Armanet et al., 1988; Guo and Jun, 1989), although some values reported for Cr_2O_3 (Stout, Gerberich et al., 1986) and Al_2O_3 (Luthra and Briant, 1986; Diot, Choquet et al., 1989) are as high as several thousand MPa. There are very few measurements of the stress that develops simultaneously in the adjoining substrate, (Stout, Gerberich et al., 1986; Diot, Choquet et al., 1989) but in general average values are an order of magnitude smaller and of opposite sign. Efforts to estimate the growth stress by subtracting the

calculated thermal stress from the measured residual stress have been made. The mathematical models used to calculate the thermal stress are simplistic; they do not account for complicating issues such as creep in the oxide and metal or scale fracture, and they are also dependent on reliable material properties of the oxide and metal. A comprehensive understanding of stresses, and how they develop with time, requires independent determination of the growth and thermal stress components, which can only be made *in-situ*, during the oxidation process.

Experimental System

The X-ray system used in this study employs the transmission diffraction geometry. The transmission method has several advantages over traditional reflection techniques such as the $Sin^2(\Psi)$ method. The transmission technique provides a means of making rapid *in-situ* determinations of elastic in-plane lattice strains in both the oxide and underlying metal; the $Sin^2(\Psi)$ method has been predominantly restricted to measurements in the oxide. The transmission geometry also provides an average measure of the strain throughout the entire sample; reflection techniques measure only the strain at the surface of the sample. The transmission technique therefore provides a more representative average measurement of the strain in the oxide and metal.

The primary components of the X-ray system are depicted in **Figure 1**. The X-ray source is a Rigaku RU-200 generator with a Mo rotating anode. The generator is run at 50 kV and 15 mA yielding a primary beam of 750 Watts. The primary beam is monochromated using a quartz crystal focusing monochromator. The monochromator eliminates the Mo Kβ peaks, and clearly resolves the Mo $K\alpha_1$ and Mo $K\alpha_2$ peaks. The monochromated beam is collimated with a 500 μm gold pinhole aperture.

The specimen is placed at the center of a rotatable ceramic stage and is supported between two sheets of mica. A hole drilled through each mica sheet forms an aperture allowing exposure of the specimen to the beam. The specimen is heated with an electric resistance furnace which is placed over the specimen stage. The furnace, which has a maximum temperature of 1100°C, is constructed of Kanthal™ A1 heating elements and high-grade Al_2O_3 ceramics. A 2 mm hole in the side of the furnace allows the beam to impinge on the sample. The diffracted and direct beams exit through a slit on the opposite side of the furnace. The furnace temperature is controlled by a low voltage programmable temperature controller. The control gas is delivered at the top of the furnace and is exhausted through the X-ray entrance and exit ports. A curved-wire position sensitive detector (PSD) is used to collect the diffraction spectrum. The spectral output of the PSD is processed by a Tracor Northern 1710 multichannel analyzer.

Experimental Procedure

A typical experiment consists of three phases: heating, isothermal oxidation, and cooling. During the heating phase the temperature is raised to the desired oxidation temperature in steps using a programmable temperature controller. At each temperature step the temperature is allowed to equilibrate and a diffraction spectrum is taken. A non-oxidizing atmosphere, typically N_2-10%H_2, is maintained in the furnace during this phase to avoid oxidation. Consequently, only thermal expansion of the metal is measured. Once the desired temperature is reached the oxidation phase is initiated by introducing pure oxygen into the furnace. The diffraction information is continuously collected and stored as oxidation progresses over several hours. The growth strain, if any, will be observed during this period. After the desired oxidation time the cooling phase is initiated. The temperature is reduced in steps, and a diffraction spectrum is taken at each step to monitor the thermal strains generated on cooling.

The lattice spacing, d, for each (hkl) reflection is calculated from the diffraction peak centroid using Bragg's law. The lattice strain is calculated using the familiar equation:

$$\%\varepsilon = \frac{(d-d_o)}{d_o} \cdot 100$$

where d_o is the unstrained ASTM lattice spacing.

Experimental Results and Discussion

The *in-situ* X-ray diffraction system has been successfully employed to measure the strain during all phases of the oxidation process - heating, isothermal oxidation, and cooling in the simple systems of Cr/Cr_2O_3 and Ni/NiO. The *in-situ* strain measurements on the oxidation of Cr and Ni have provided a wealth of information which would not otherwise be available from residual strain measurements. The strain measurements suggest that the strain state in the oxide and metal is a complex function of the oxide morphology, crystalline texture and the substrate orientation. The growth stress, which has often been disregarded in residual stress experiments, can influence the residual strain state of the oxide and metal.

OXIDATION OF NI

The strains observed during the oxidation of a 25 μm Ni foil are presented in **Figure 2**. Upon heating in N_2-10%H_2 the annealed Ni foil expands 1.6%, slightly greater than the expected thermal expansion value of 1.5% predicted in the literature (dashed line). Shortly after introduction of O_2 the oxide, NiO, is observed; simultaneously an increase in tensile strain of approximately 0.8% is observed in the metal. This strain is equal to the (elastic) strain at yielding of the metal.

The metal and oxide strains remain relatively constant during the isothermal oxidation period. The oxide is also in tension relative to its normal thermal expansion strain of 1.3% (dashed line).

Prior to these measurements it was thought that the oxide and metal strains developed gradually over time; however, our measurements show that the strain develops very rapidly after introduction of O_2. Over the volume of the specimen the forces from the stresses must be balanced, i.e., nominally the oxide is in compression and the metal experiences tension. However, a tensile oxide strain is observed experimentally. The NiO scale has a duplex structure: a fine-grained equiaxed interior zone, and a columnar exterior zone. One possibility is that the growth mechanisms of the two zones may induce different signs of growth stresses. The exterior zone exhibits a crystalline texture, which will affect diffraction intensities. This tensile strain may be the result of preferential diffraction from a portion of the oxide scale. The interior equiaxed zone is randomly oriented and as such some portion of the scale is always in diffracting condition. The measured strains may therefore be dominated by the strain representative of the interior equiaxed zone. A similar observation of a duplex stress state has been made by (Ueno, 1974).

The residual strains, measured at room temperature, suggest that the oxide and metal are both in a state of compression. The metal, however, is in tension relative to the initial unoxidized strain state. The *in-situ* measurements show that the elastic strain limit in the metal was reached during the isothermal oxidation period. These strains are maintained upon cooling to room temperature, thus demonstrating that a simple subtraction of a calculated thermal stress from the measured residual stress does not provide a realistic measure of the growth stress. The experiments also suggest that the initial strain state of the metal, prior to oxidation, can effect the interpretation of the final strain state of the system, an aspect which has been heretofore neglected in residual stress measurements.

The dependence of strain state on oxide and metal thickness was investigated by oxidizing foils of various thickness. The oxidation strain profile for a 125 μm Ni foil is presented in **Figure 3.** The thicker metal foil exhibits no significant increase in strain during the isothermal oxidation period; the oxide strain is compressive during this period. While the metal strain may be substantial at the metal/oxide interface, the average metal strain is distributed over a greater volume of metal than the 25 μm foil, reducing the average measured strain. The residual metal strain is also zero, the residual oxide strain remains in compression. The importance of crystalline texture is again illustrated by the absence of the NiO (220) and (200) reflections; suggesting that the measured oxide strain may not be representative of the entire oxide scale.

In-situ experiments on the oxidation of Ni to date suggest that the residual stress in the oxide and metal is a complex function of the growth and thermal stresses. Theses stresses are influenced by the oxide morphology, crystalline texture and the initial stress state of the metal.

OXIDATION OF Cr_2O_3

Oxidation studies on Cr have been confined to single crystals due to a lack of high quality polycrystalline materials. The single crystal experiments provide a unique opportunity to study the effect of crystal orientation on the stress state of the system. Initially experiments were performed on single-crystal Cr oxidized on the (100) face. These experiments have been extended to examine the effect of substrate thickness on the state of stress. Experiments on the oxidation of the Cr (111) face have also been carried out to establish the effect of crystal orientation on the stress state of the system.

Typical results for Cr oxidized on the (100) face are illustrated in **Figure 4**. A small tensile strain in the metal (relative to the unstrained thermal expansion strain) is observed once the oxidation temperature is reached, but before oxygen is introduced. This strain is believed to result from a thin oxide layer formed during heating due to the incomplete suppression of oxidation. Upon introduction of O_2 an increase in tensile strain is immediately observed in the metal. The oxide, which is observed shortly after the introduction of oxygen, develops a tensile strain relative to the unstrained thermal expansion value. Each of the oxide reflections exhibits a different thermal strain at the oxidation temperature. The (11•0) and (10•4) reflections are in tension, the (11•6) is in compression. As oxidation proceeds the strain in both the oxide and metal remain relatively constant. Upon cooling the metal maintains a residual tensile strain. The (11•0) Cr_2O_3 reflection exhibits a small tensile residual strain. This is also the direction of greatest thermal expansion and the most elastically compliant direction in the hexagonal crystal structure. The (10•4) and (11•6) Cr_2O_3 reflections exhibit a residual compressive strain. These two planes have a lower thermal expansion than the (11•0), and are elastically stiffer than the (11•0).

Oxidation experiments on Cr single-crystals oxidized on the (111) face are summarized in **Figure 5**. Again, the metal exhibits a small tensile strain increase immediately after introduction of O_2 into the system. The oxide strain maintains both tensile strains in the (11•6) reflection and compressive strains in the (11•0) and (10•4) reflections. The metal maintains a residual tensile strain on cooling. A residual compressive strain is measured in each of the three oxide reflections.

Almost all of our previous experiments, including the most recent ones, indicate that growth stresses developed in both metal and oxide are constant during the isothermal oxidation period. The growth stress appears to be independent of scale thickness.* This suggests that the growth stress in the Cr/Cr_2O_3 system reaches a threshold at which some relaxation process, such

---

* Earlier theoretical studies, which did not take into account oxide growth mechanisms, suggested that the magnitude and distribution of stresses in the metal and oxide would depend on the ratio of metal/oxide thicknesses.

as creep or yielding, determines the stress state. The mechanism of relaxation merits further experimental studies, and theoretical modeling studies are presently considering this issue

The complex nature of the stress state is exemplified by the variability in the oxide strain with crystalline direction. While the metal strain is consistently tensile, both compressive and tensile strains have been observed in the oxide. The oxide strains are believed to result from variations in oxide texture, metal substrate orientation and the anisotropic behavior of the thermal expansivity and elastic modulus of the oxide. The results obtained to date illustrate the complex evolution of stresses during the oxidation period and the important influence of the growth stress on the residual stress. A determination of the residual stress alone reveals little about the stress state encountered during oxidation.

II OBSERVATIONS OF SCALE FRACTURE BY ACOUSTIC EMISSION

Under practical oxidizing conditions, stresses induced by the scale growth process and particularly by thermal expansion mismatch during thermal cycling may be sufficient to cause cracking and spalling of the protective oxide scale. (Stringer, 1970; Hancock and Hurst, 1974; Baxter and Natesan, 1983) Some work has been done to identify practical ways of improving the oxide scale adherence to the metallic substrate, (Stott, 1988), and to identify the basic factors that determine the scale cracking/spalling process. (Evans, 1988; Evans, 1989)

Oxide scales formed on different metals or alloys behave differently with regard to their resistance to spallation. Some of them have very good resistance to cracking and spalling, e.g., the MCrAlY - type alloys, some do not. The oxide scale formed on 304 stainless steel is an example of one that is easy to crack and spall, therefore it has been chosen here as a model of cracking and spalling processes. Acoustic emission has been applied to investigate the fracture process of oxide scales formed on 20Cr-25Ni-Nb stabilized stainless steel, (Evans, 1988; Bennett, Buttle et al., 1989) but no similar study of the behavior of 304 stainless steel scales has been found. The purpose of this work is to study the fracture of the oxide scales formed on 304 stainless steel.

Experimental Procedure

The acoustic emission technique (AE), which is a very useful tool in the study of the fracture of brittle materials,* was used to monitor scale cracking and spallation during experiments involving isothermal oxidation and subsequent controlled cooling to room temperature. SEM was used to characterize the scale cracking morphology and spalled regions on the oxide scale.

---

* (Desai and Gerberich, 1975; Huang, Lin et al., 1984; Khanna, Jha et al., 1985; Jha, Raj et al., 1986; Khanna, Jha et al., 1986; Christl, Rahmel et al., 1987; Bennett, Buttle et al., 1989)

Samples of 304 stainless steel* were cut from a bar into disks 9.5 mm diameter and 0.5 mm in thickness. The surface of the samples were polished through 600 grit silicon carbide paper. The sample is spot-welded to a platinum wire and suspended in the oxidation chamber. The platinum wire also acts as the acoustic signal waveguide. A schematic of the experimental setup is presented in **Figure 6**.

The samples were isothermally oxidized at 800°C for 20 hours in pure O_2 flowing at 50 cc/minute, then furnace cooled to some intermediate temperature and held at that temperature for 24 hours before being cooled to room temperature. After the initial isothermal oxidation period the reaction chamber was flushed with Ar to suppress further oxidation. Acoustic emission signals generated at the surface of the sample are transmitted to the AE transducer by the Pt waveguide, amplified to a total gain of the 95.6 dB and subsequently processed using the AET 5000 system.

Results and Discussion

After 20 hours isothermal oxidation at 800°C in flowing pure oxygen, a scale about 10 μm thick, containing Cr_2O_3 and spinels, formed on the sample. In all the experiments, only a few (insignificant number) AE events were recorded during the isothermal stage, indicating that the growth stress is not large enough to fracture the scale. **Figure 7** shows the AE result of an experiment in which the sample was furnace cooled directly to room temperature. In this experiment, the scale started to crack and spall continuously when the sample was cooled to a relatively low temperature (about 300°C). Since the thermal stress is approximately proportional to the cooling amount (ΔT),(Tien and Davidson, 1974) it appears that a certain level of stress is needed to start the scale fracture process. As cooling continued, the amount of cracking and spalling (as represented by the rate AE events) kept increasing to a peak value at approximately 150°C , then decreased to very low level when the temperature reached room temperature. It should be noticed, however, that even after the sample was at room temperature, additional AE events were detected, although no additional stresses were applied to the specimen. One possible explanation is that some cracks continued to grow slowly under the static stress until they reached critical size for fracture.

For other experiments, cooling was interrupted for 24 hours at various temperatures between 300°C and room temperature. **Figure 8** shows the results of an experiment in which the sample was held at 200°C for 24 hours. It can be seen that AE events were initiated at approximately 300°C, as before, but the events stopped shortly after the temperature stabilized at 200°C, implying that the scale fracture process had been almost stopped. Small numbers of AE

---

* The nominal composition of 304 stainless steel is 18.0-20.0% Cr, 8.00-10.50% Ni, <2.00% Mn, <0.045% P, <0.030% S, <1.00% Si, 0.08% C, balance Fe.

events were recorded during holding, indicating the possibility of slow crack growth during this period. When cooling was resumed after 24 hours, additional large numbers of events were recorded, giving rise to a steep peak, indicating that the extensive scale cracking and spalling started again at a small additional ΔT. **Figure 9** shows the results of a 100°C holding experiment, and again the AE events were suspended during the hold period. It should be noticed that 200°C is low enough to suppress substrate creep. Therefore scale cracking and spalling will be the only way of releasing stresses.

Since cracking and spalling of the scales continued over a range of temperature, no single critical fracture stress applies to the entire specimen, in agreement with the proposal by (Evans, 1988). As Evans suggested, the entire scale may be viewed as many small regions, some of them are easy to fracture, some are not. At some critical stress level (associated with ΔT), the weakest regions will spall away, some regions will crack, and some regions remain intact. The stress will be completely relaxed in the spalled area, partially relaxed in the cracked area, and completely sustained in the intact regions. These features are shown in **Figure 10**, an SEM micrograph of an oxidized 304 stainless steel. This analysis shows that the oxide scale structure is not homogeneous throughout the entire sample, and therefore the scale will fracture over a range of stresses, associated with a range of ΔT.

From the experimental results it can be seen that the growth stress may not play a significant part in the scale fracture process since only a very small number of AE events were recorded during the isothermal oxidation stage. However, the small number of cracks produced in that stage could act as the nuclei for later cracking and spallation during cooling. The continuation of cracking, after the specimen has reached a constant temperature and therefore is in a state of static or diminishing stress, is not well understood. One possibility is that some existing cracks (flaws) may continue to propagate slowly under the remaining stresses. A few such cracks may reach critical size, triggering a few cracking events. When cooling is resumed, the increased stress will activate a much larger number of near-critical size flaws, producing additional AE events.

The model of the cracking and spallation processes, alluded to above, which is based on ΔT generating a stress that rises to the local fracture stress is somewhat naive. First, the stress directly related to ΔT is biaxial and strictly applies at a flat metal/oxide interface. In reality, the stresses are likely to be triaxial, and the stress in the thickness dimension may be a crucial component of the fracture stress. Such considerations will be particularly important near edges, corners and non-planar interfaces. Secondly, as shown in the preceding section, the magnitude of the local stress also depends on the crystallographic orientations of the metal and oxide and the relationships between crystal directions and elastic moduli of the metal and oxide. Thus while an average stress may be readily calculated, the magnitude of the local stress may deviate considerably from the average. Thirdly, since the oxide is a brittle material, the fracture stress of a local region

will be controlled by the size of local flaws. Such flaws may include scale morphology features, such as grain boundaries or static crack tips. Fourthly, the interaction between adjacent regions would seem to be important and quite complicated. On the one hand, a fracture in one region may introduce a larger flaw (the advancing crack tip) in an adjacent region. This would have the effect of allowing fracture in the adjacent region at a lower stress. On the other hand, cracking and spalling invariably lowers the local stress in the region experiencing the crack, but the reduction of stress there may also allow a relaxation of the stresses in adjacent regions. Thus cracking events in adjacent regions may be expected to be interdependent. Fifthly, as noted above, cracking can be time dependent at a fixed stress. The foregoing discussion suggests some factors to be considered in the development of a model not yet expressed in mathematical terms. The concept of viewing the oxide scale as comprised of a field of small regions or cells, each described in terms of a pre-existing flaw, a state of stress dependent on temperature and crystal orientation and a mechanical connection (interaction) to adjacent regions seems like a fruitful approach. A deterministic solution of such a problem is probably not feasible because of the difficulty of specifying structural and morphological parameters. However, the large number of cracking events invites a statistical approach to solving such a problem. This is an issue we will continue to pursue in the coming year.

III MODELING OF GROWTH STRESS IN A THIN METAL PLATE DUE TO HIGH TEMPERATURE OXIDATION

The objective of this study is to model the distribution of stresses in an adherent oxide scale and its metal substrate and to describe the evolution of these stresses with time as the scale grows isothermally. The Cr/Cr_2O_3 system was chosen to provide explicit calculated values for comparison with experimental *in-situ* X-ray measurements. As the scale grows at the oxidation temperature, the misfit between the scale and the metal substrate is a source of strain, some of which may be accommodated by free expansion into the gas phase and some is accommodated by inducing stresses in the scale and substrate. These stresses are subject to partial relaxation by plastic deformation, i.e., yielding if the stress is high enough, and by creep at lower stresses. Thus, as the scale grows, it may be expected that the stresses will evolve in a complicated manner. This work builds upon and extends an earlier study in which the source of strain (at a fixed scale thickness) was the thermal expansion misfit between the scale and metal upon cooling (Barnes, Goedjen, et al., 1989).

Mechanical Equilibrium and Deformation of the System

Since the Cr samples used in the X-ray diffraction experiments are thin flat plates and the measurements are focussed on the middle portion of the plate to avoid edge effects, a geometrically simple model, as illustrated in **Figure 11a** can be used. The mechanical force balance of the system, as illustrated in **Figure 11a**, requires:

$$\frac{d}{dt}\left[\, \sigma_{ox}(t)\, b_{ox}(t) + \sigma_{sb}(t)\, b_{sb}(t) \,\right] = 0$$

where t is time, b_{ox} and b_{sb} denote the oxide and substrate thickness, respectively. In expanded form,

$$\dot{\sigma}_{ox}\, b_{ox} + \dot{\sigma}_{sb}\, b_{sb} + \dot{b}_{ox}\, \sigma_{ox} + \dot{b}_{sb}\, \sigma_{sb} = 0$$

For Cr_2O_3, the rate of stress growth and relaxation is given by Hook's law

$$\dot{\sigma}_{ox} = H_{ox}\, \dot{\varepsilon}^{e}_{ox} = (\, \dot{\varepsilon} - \dot{\varepsilon}^{vp}_{ox}\,)$$

where H_{ox} is the biaxial elastic modulus defined by

$$\bar{H}_{ox} = \left[\, \frac{E}{1-\nu} \,\right]_{ox}$$

$\dot{\varepsilon}^{vp}_{ox}$ is the visco-plastic strain rate, and $\dot{\varepsilon}$ is the overall in-plane strain of the system. The total accumulated stress also depends on the misfit strain ε^{*}_{sb} between the scale and the substrate:

$$\sigma_{ox} = H\,(\, \varepsilon - \varepsilon^{vp}_{ox} - \varepsilon^{*}_{sb})$$

The misfit strain is defined as:

$$\varepsilon^{*}_{sb} = \frac{(PBR - 1)}{3}$$

where PBR is the Pilling-Bedworth Ratio. For Cr, the total stress is only dependent on the elastic strain

$$\sigma_{sb} = H (\varepsilon - \varepsilon_{sb}^{vp})$$

The creep of Cr and Cr_2O_3 are assumed to be described by the power-law mechanism defined by

$$\dot{\varepsilon}^{vp} = A \frac{\mu b}{kT} D (\frac{\sigma}{\mu})^n$$

where A and n are constants, μ is the shear modulus, b is Burger's vector, T is temperature and D is the self-diffusion coefficient. To calculate $\dot{\varepsilon}$ and $\dot{\sigma}$ the growth rate of the scale must also be specified. The parabolic growth equation is used to model the scale growth rate for the Cr/Cr_2O_3 system

$$\dot{b}_{ox} = \frac{K_p}{b_{ox}}$$

where K_p is the parabolic rate constant. The recession of the Cr/Cr_2O_3 interface can be calculated from the PBR of the system and the misfit strain defined above.

RESULTS

The Runge-Kutta scheme is employed to numerically integrate the rate equations for scale growth and the visco-plastic strains and stresses. In particular, the oxidation of a thin Cr plate, 2 mm thick, at 1200°C and 1400 °C, was considered using the data for scale growth from (Birks and Meier, 1988) and the power-law creep data from (Frost and Ashby, 1982). These high temperatures were selected for a preliminary evaluation of the role of creep during oxidation. The calculated stress relaxation in the scale and the scale thickness are plotted in **Figure 11b.**

Relaxation of the compressive stress in the scale occurs within 10^5 seconds (27.77 hr) during oxidation for both temperatures. As discussed by (Frost and Ashby, 1982), for a ratio of shear stress to shear modulus over 10^{-2}, the predominant deformation mechanism is controlled by dislocation glide. The broad stress range encountered during relaxation dictates that constitutive equations which account for dislocation glide be incorporated into future modeling.

IV ADHESION OF NiO ON Ni BY NANO-INDENTATION AND SCRATCHING TECHNIQUES

As discussed by (Atkinson and Guppy, 1991), there are several techniques for the measurement of the adhesion of thermally grown oxide scales to their substrates. However, none of them is capable of determining the true fracture toughness of the interface. For scale layers less

than 10 μm thick, micro-hardness indentation and scratching tests were used to obtain the information on metal/oxide adhesion (Atkinson and Guppy, 1991). For scale layers less than 1 μm thick, no such measurements have been reported. (Venkakaraman and Gerberich, 1992) have examined the work of adhesion between the film and substrate for the Cr/Al_2O_3 thin film system using the nano-scratching test technique.

In the present study the nano-indentation technique has been applied to a 5 μm thick NiO scale grown on pure Ni (oxidized for 30 min in O_2 at 900°C and air cooled to room temperature). The purpose was to measure the interfacial fracture toughness of the metal/oxide interface. The indentation and scratching tests on this sample were performed using the Nano-Indentor® equipment at room temperature. A conical indenter with a tip curvature of approximately 5 μm is first driven vertically into the NiO scale. As seen in this SEM micrograph, **Figure 12**, the indentation causes severe plastic deformation of the Ni substrate and fracture of the scale along the oxide grain boundaries. The scale has a duplex structure with an exterior columnar scale with grains 1.5 μm in diameter, and an equiaxed interior oxide.

An SEM micrograph of two scratch tracks from the indentor tests performed on the same sample are shown in **Figure 13**. Track (A) is from a scratch made with a maximum load 0.12 N to a depth of 1.5 μm into the scale, the lower scratch was made with a maximum load 0.22 N to a depth of 2.7 μm. Mode I cracking of the scale is clearly seen within the scratch running perpendicular to the scratch direction. Oxide spallation has occurred on the lower track (deeper scratch) exposing the interior layer of the duplex oxide structure. These results will be quantitatively analyzed to characterize the fracture properties of the metal/oxide system. Further tests will be performed on the Ni/NiO and other systems with various scale thicknesses using indentors with smaller tip curvature.

REFERENCES

Atkinson, A. and R. Guppy (1991) Materials Science and Technology, **7**, 1031-1041.

Aubry, A., F. Armanet, G. Beranger, J.L. Lebrun, et al. (1988) Acta Metallurgica, **36**, 2779.

Barnes, J. J., J. G. Goedjen and D. A. Shores (1989) Oxidation of Metals, **32** 449-469.

Baxter, D. J. and K. Natesan (1983) Review of High Temperature Materials, **5**, 149-250.

Bennett, M. J., D. J. Buttle, P. D. Colledge, J. B. Price, et al. (1989) Materials Science and Engineering, **A120**, 199-206.

Birks, N. and G. H. Meier (1988) "Introduction to High Temperature Oxidation of Metals", E. Arnold ed.,

Christl, W., A. Rahmel and M. Schutze (1987) Materials Science and Engineering, **87**, 289-293.

Desai, J. D. and W. W. Gerberich (1975) Engineering Fracture Mechanics, **7**, 153-165.

Diot, C., P. Choquet and R. Mevrel (1989) "International Conference on Residual Stresses", S. D. G. Beck ed., Elsevier Applied Science, London,

Evans, H. E. (1988) Materials Science and Technology, **4**, 415-420.

Evans, H. E. (1989) Materials Science and Engineering, **A120**, 139-146.

Frost, H. J. and M. F. Ashby (1982) "Deformation-Mechanism Maps" Pergamon Press, New York.

Guo, Z. J. and Z. Y. Jun (1989) Materials Science and Engineering, **A120**, 245.

Hancock, P. and R. C. Hurst (1974) "Advances in Corrosion Science and Technology", M. G. Fontana and R. W. Staehle ed., Plenum Press, New York, 1-84.

Huang, T. T., Y. C. Lin, D. A. Shores and E. Pfender (1984) Journal of the Electrochemical Society, **131**, 2191-2196.

Jha, B. B., B. Raj and A. S. Khanna (1986) Oxidation of Metals, **26**, 263-273.

Khanna, A. S., B. B. Jha and Baldev Raj (1985) Oxidation of Metals, **23**, 159-176.

Khanna, A. S., B. B. Jha and Baldevraj (1986) Oxidation of Metals, **27**, 95-102.

Luthra, K. L. and C. L. Briant (1986) Oxidation of Metals, **26**, 397.

Pivin, J. C., J. Morvan, D. Mairey and J. Mignot (1983) Scripta Metallurgica, **17**, 179.

Stott, F. H. (1988) Materials Science and Technology, **4**, 431-438.

Stout, J. H., W. W. Gerberich, S. Lin and M. Lii (1986) "Fundamental Aspects of High Temperature Corrosion II", G. J. Yurek, D. A. Shores ed., The Electrochemical Society, Pennington, NJ,

Stringer, J. (1970) Corrosion Science, **10**, 513-543.

Tien, J. K. and J. M. Davidson (1974) "Stress Effects and the Oxidation of Metals", J. V. Cathcart ed., The Metallurgical Society of AIME, 201-206.

Ueno, T. (1974) Transactions of the Japan Institute of Metals, **15**, 167.

Venkakaraman, S. and W. W. Gerberich (1992) "Annual National Meeting of the American Ceramics Society", Minneapolis, MN,

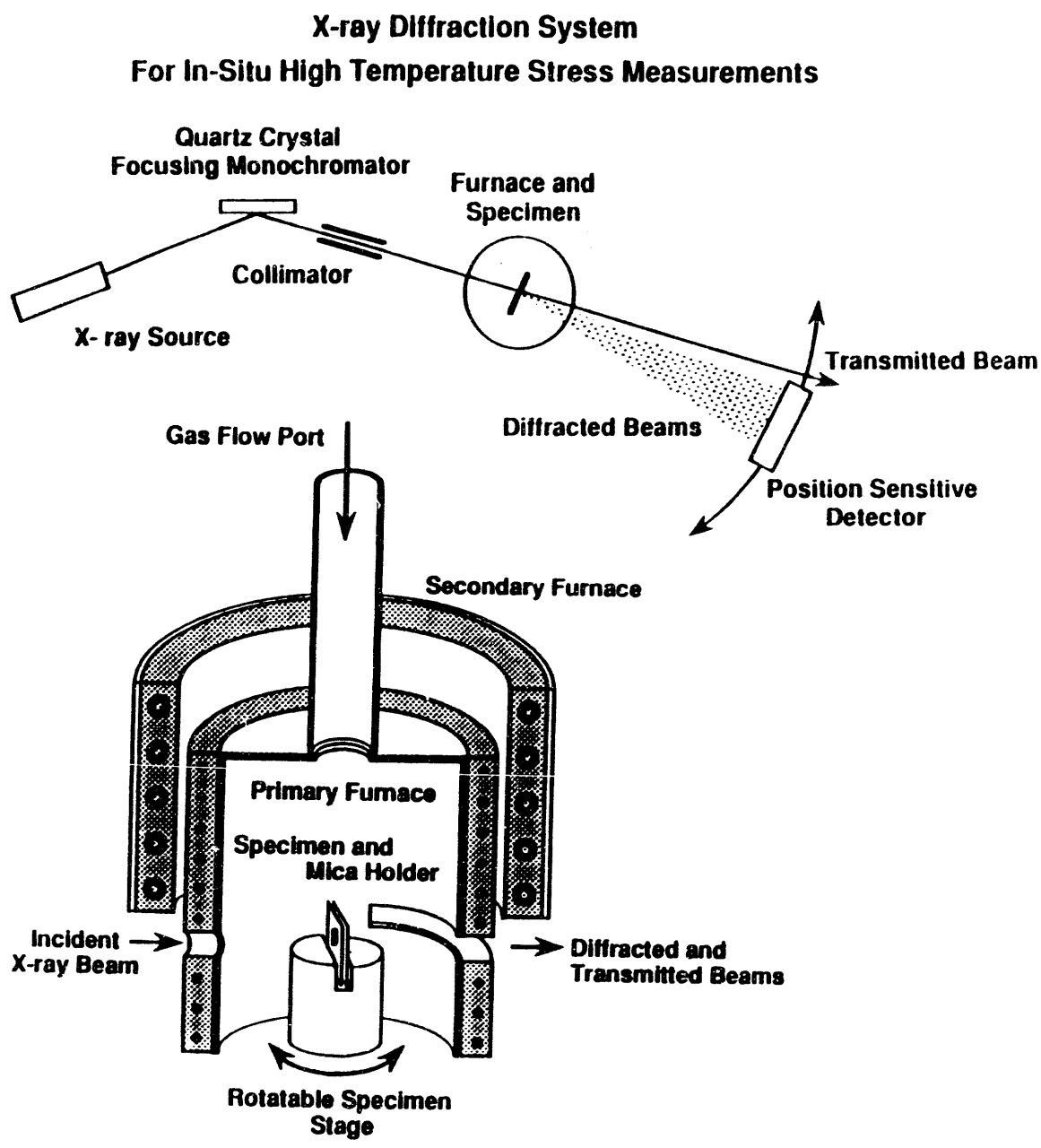

Figure 1. Schematic illustration of the *in-situ* X-ray diffraction system.

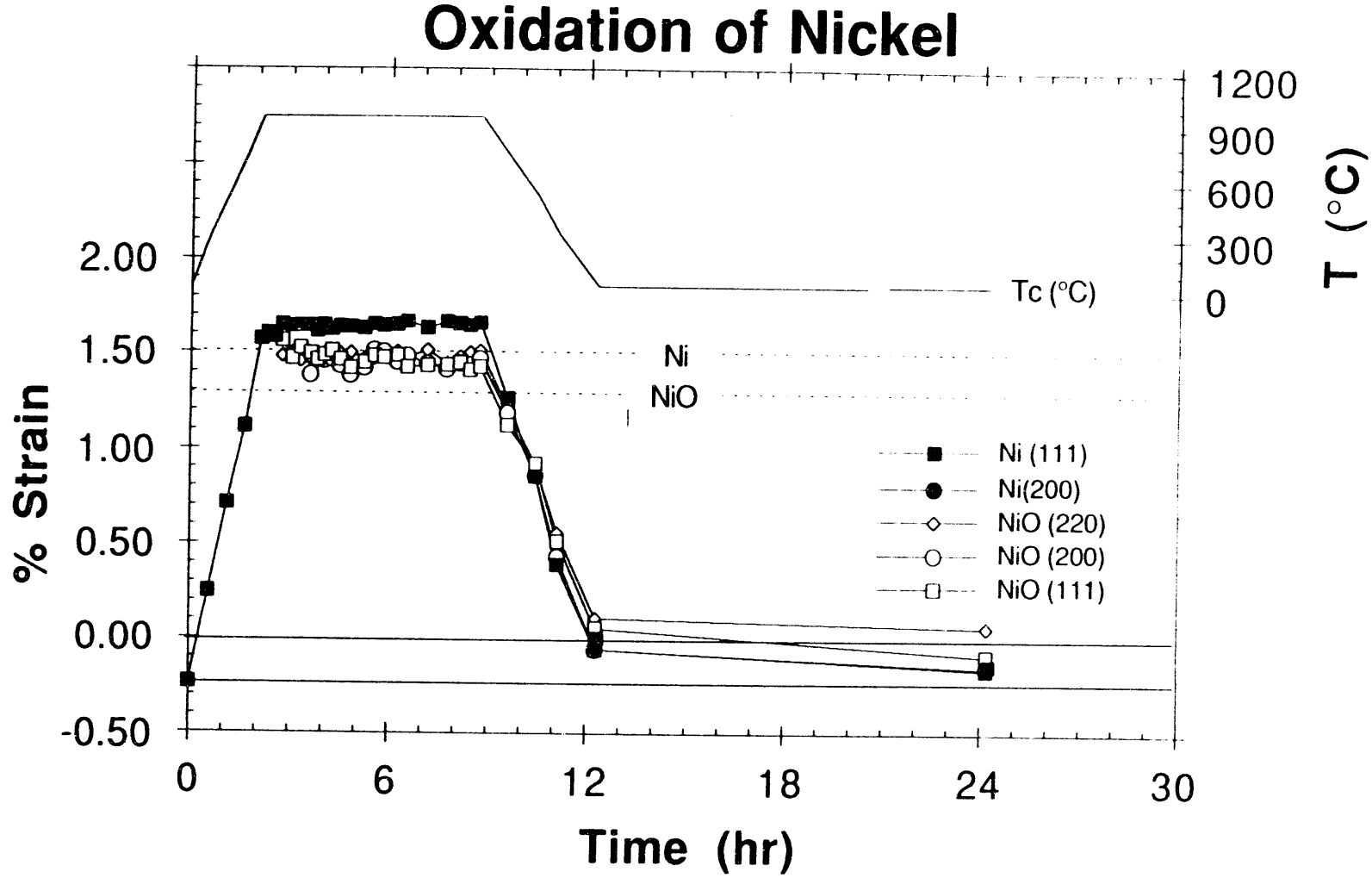

Figure 2. The strain, measured *in-situ* , during oxidation of a 25 μm Ni foil in O_2 at 940°C. The accepted literature values for thermal expansion of Ni and NiO at 940°C are indicated by the dashed lines.

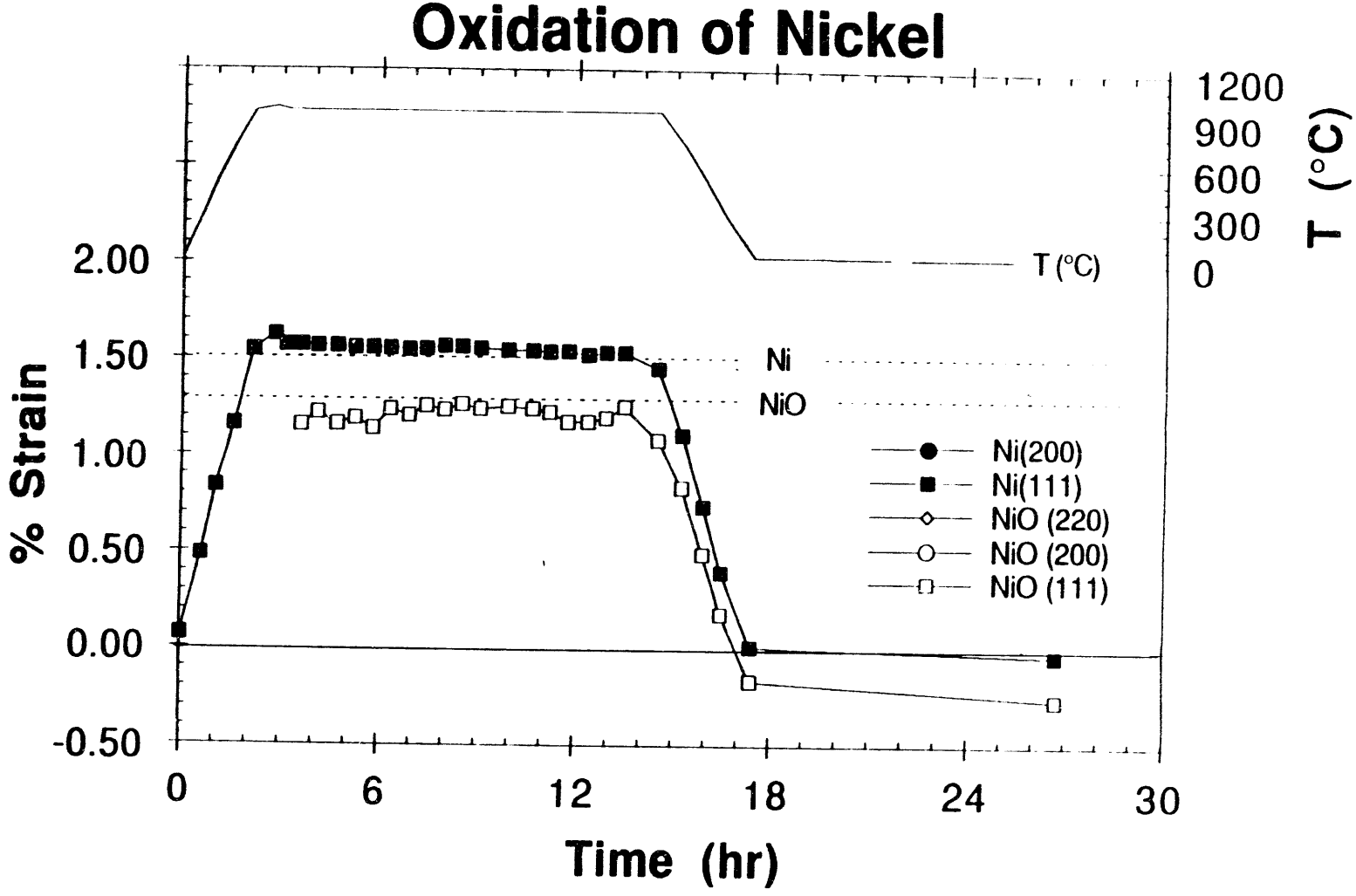

Figure 3. The strain measured during oxidation of a 125 μm Ni foil in O_2 at 940°C. The accepted literature values for thermal expansion of Ni and NiO at 940°C are indicated by the dashed lines.

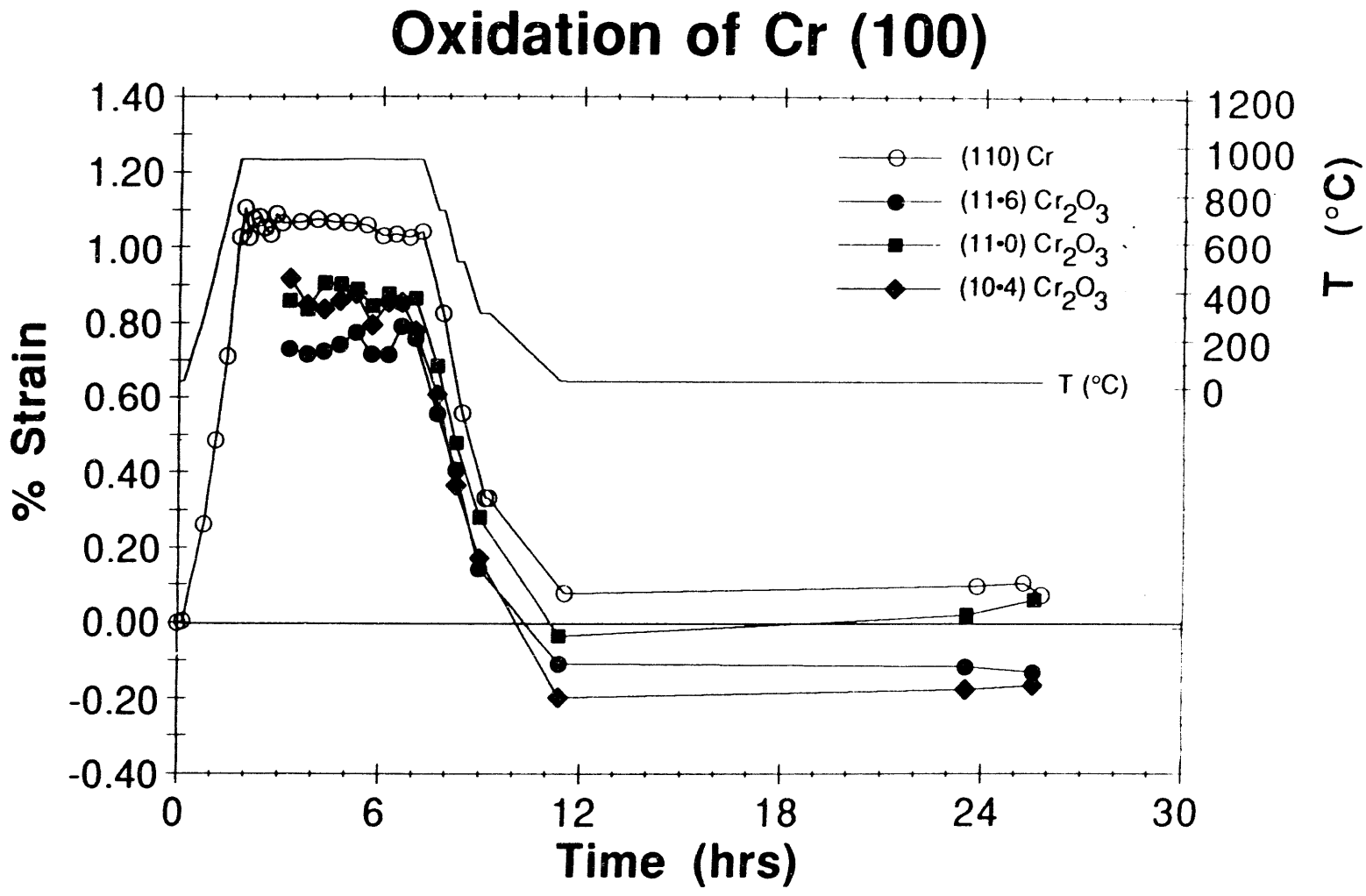

Figure 4. The measured strain during oxidation of the Cr (100) face in O_2 at 940°C.

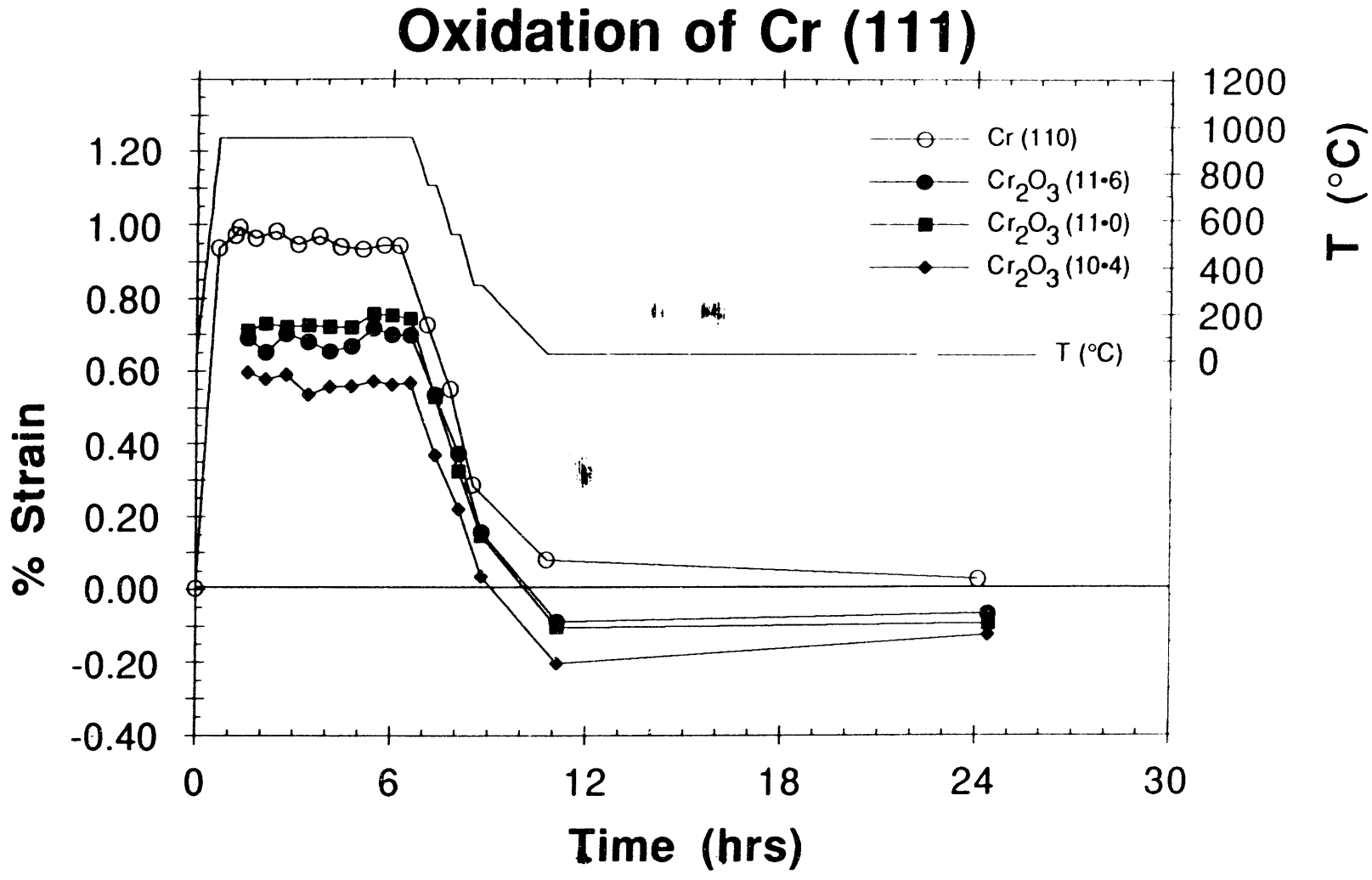

Figure 5. The measured strain during oxidation of the Cr (111) face in O_2 at 940°C.

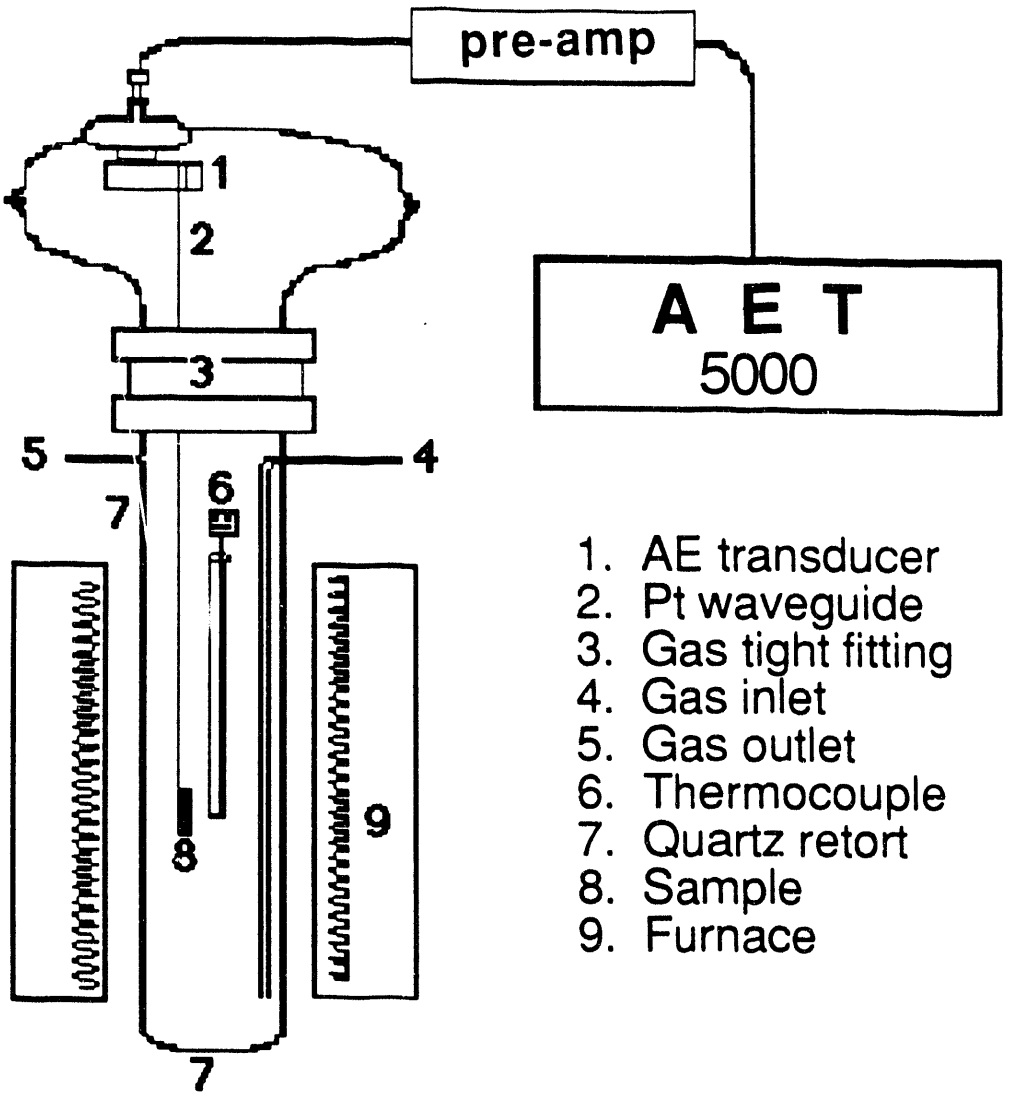

Figure 6. Schematic illustration of the acoustic emission system.

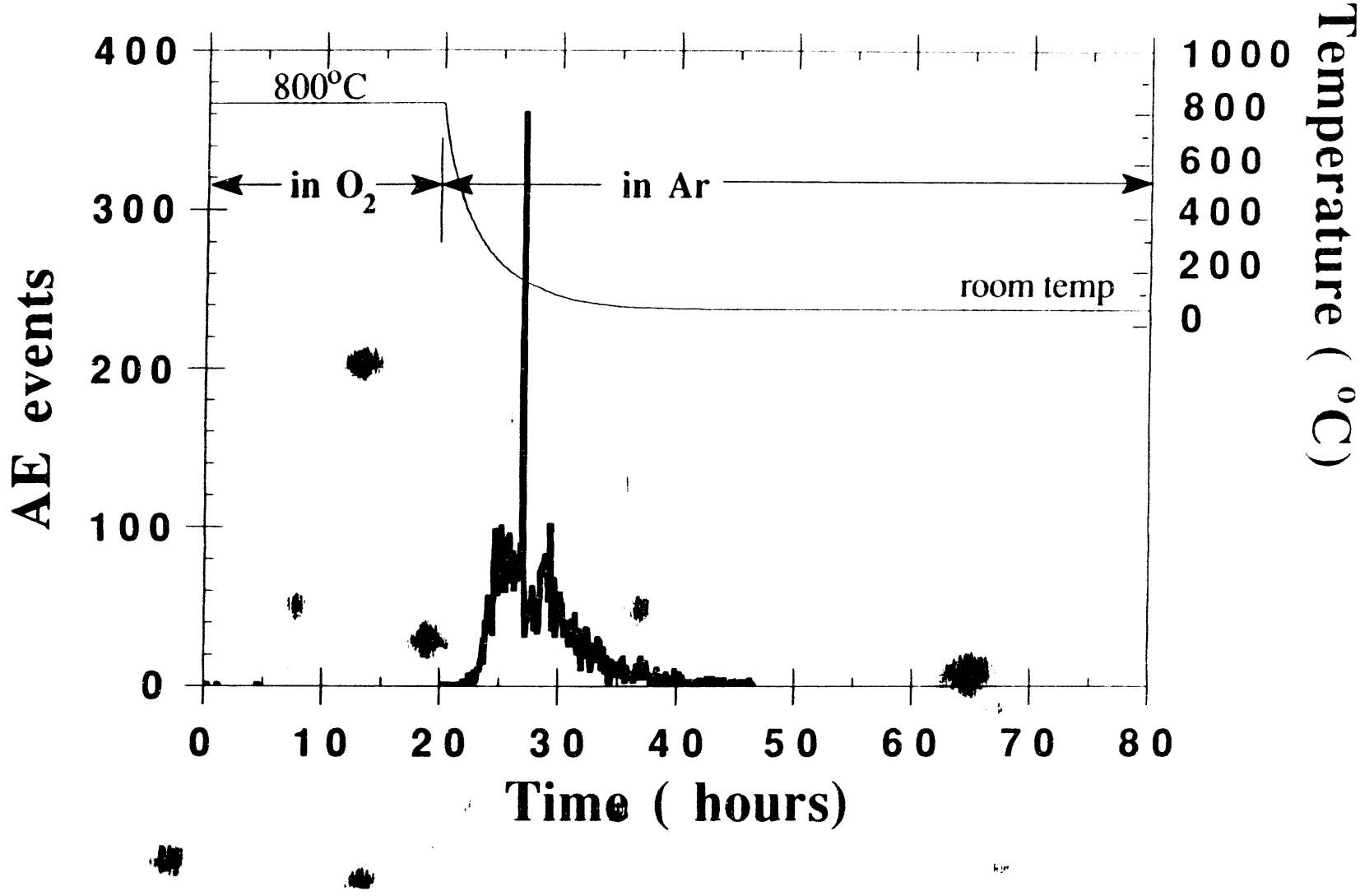

Figure 7. Acoustic emission activity observed during the oxidation and uninterrupted cooling of 304 stainless steel.

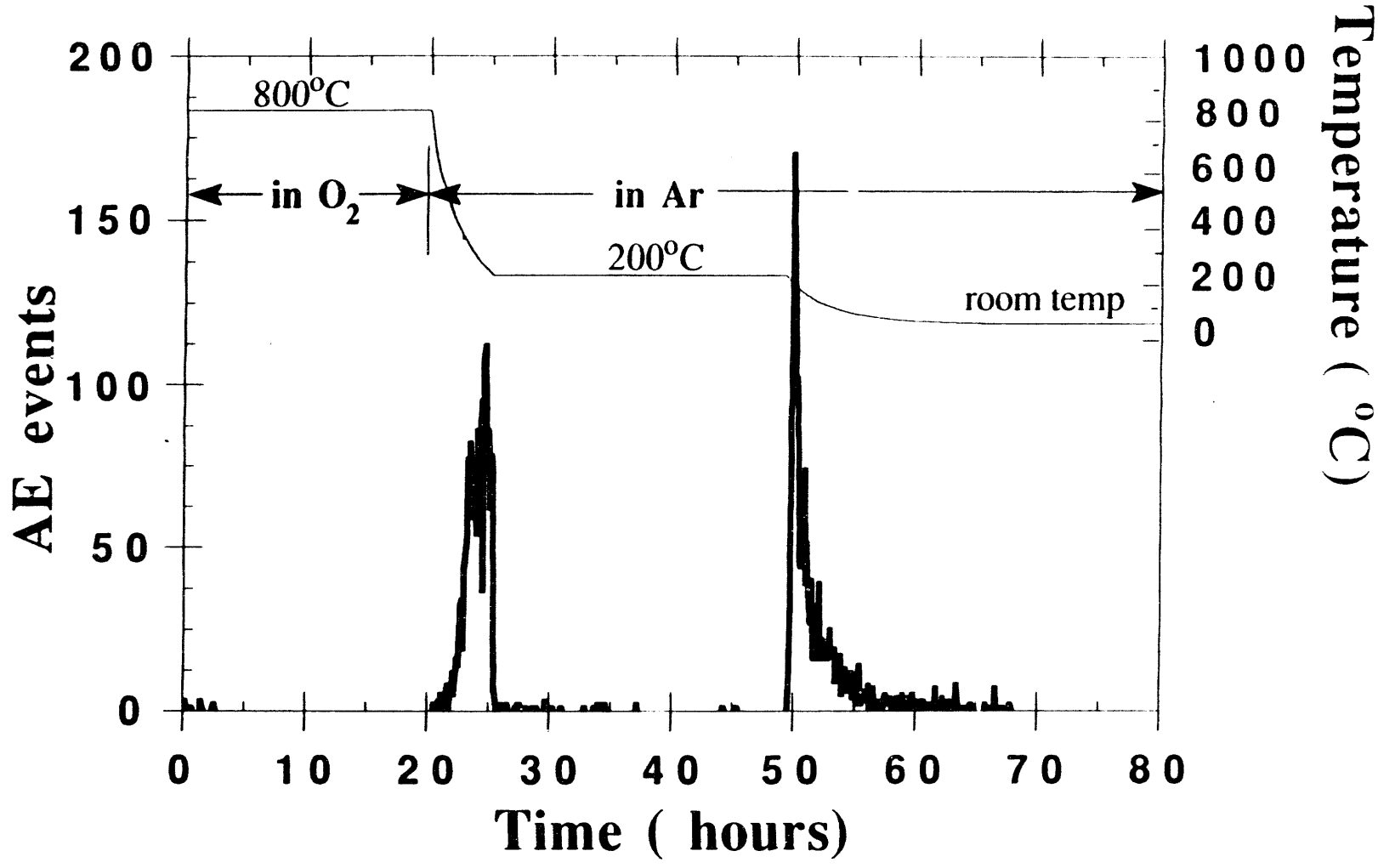

Figure 8. Acoustic emission activity observed during the oxidation and cooling of 304 stainless steel. The oxidized sample was cooled in Ar from the oxidation temperature of 800°C and held at 200°C for 24 hours before cooling to room temperature as illustrated by the superimposed temperature profile.

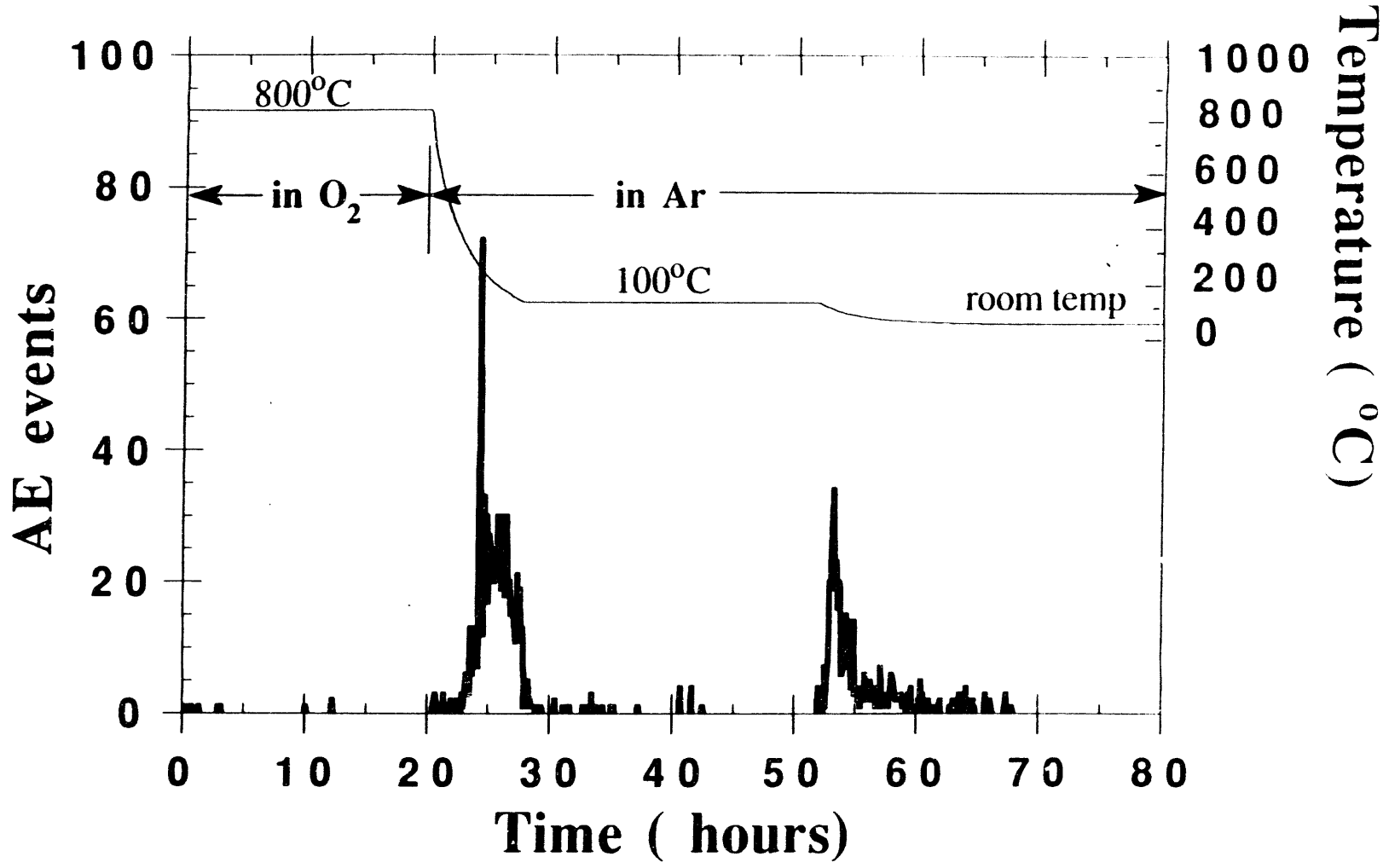

Figure 9. Acoustic emission activity observed during the oxidation and cooling of 304 stainless steel. The oxidized sample was cooled in Ar from the oxidation temperature of 800°C and held at 100°C for 24 hours before cooling to room temperature as illustrated by the superimposed temperature profile.

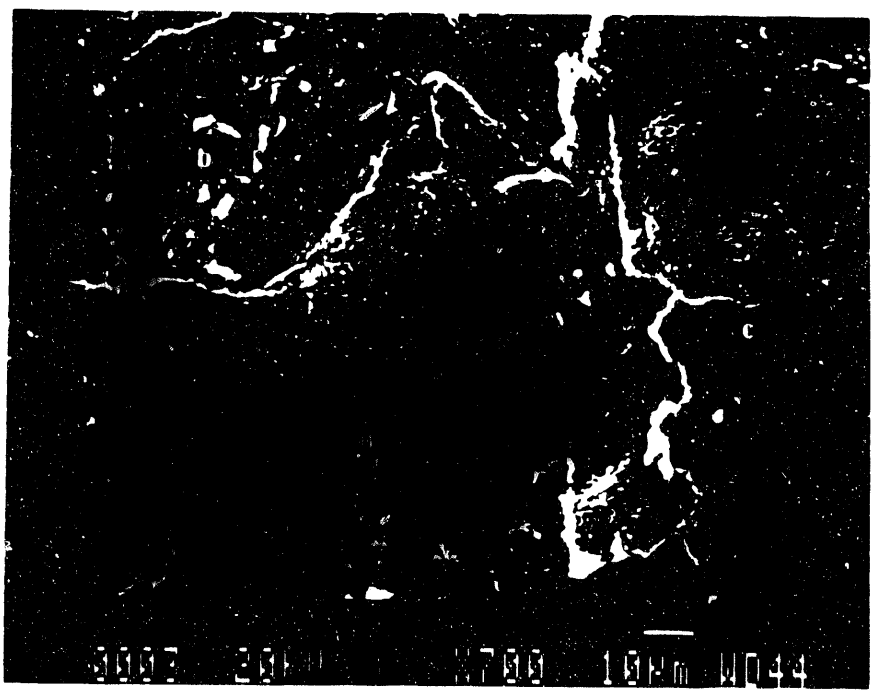

Figure 10. SEM micrograph of an oxidized 304 stainless steel illustrating the three characteristic scale regions: (a) intact (b) spalled and (c) cracked but intact. The sample was oxidized at 800°C and furnace cooled to room temperature.

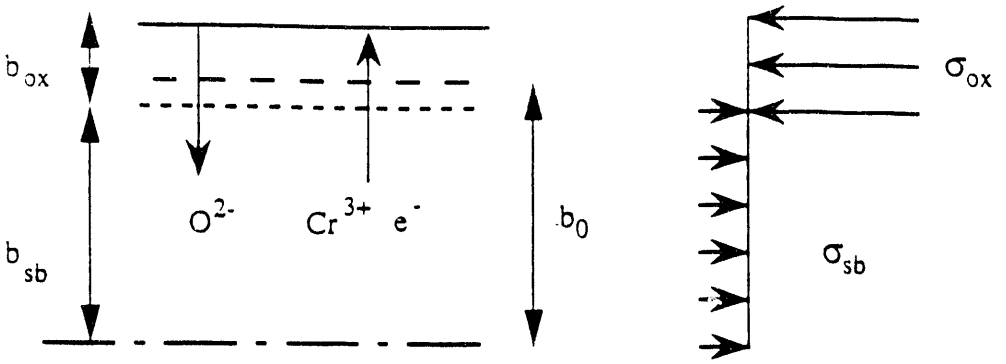

(a)

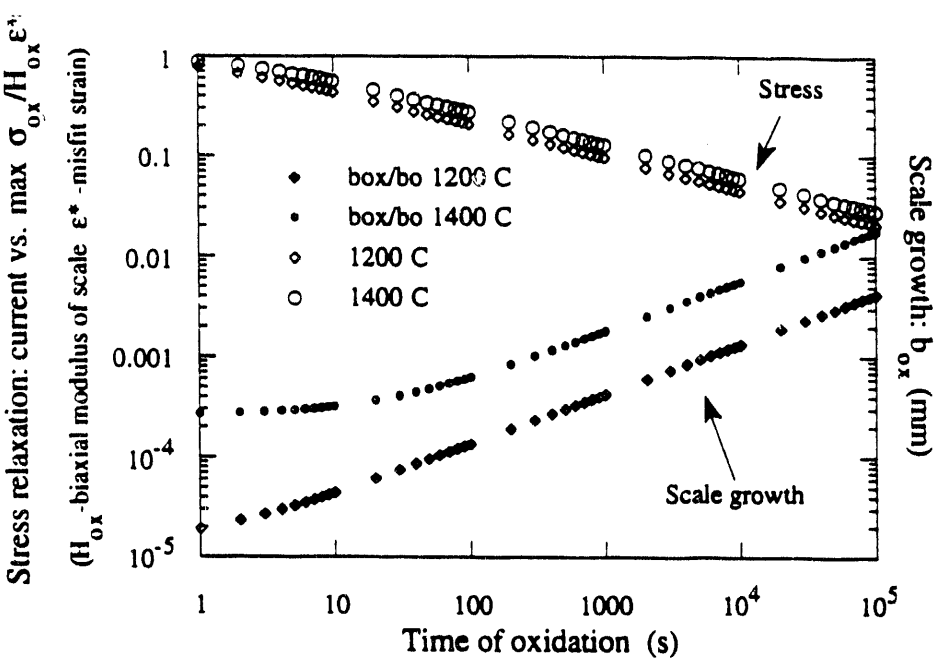

(b)

Figure 11. Schematic illustration of the oxide growth model (a). b_{ox} and b_{sb} define the oxide and substrate thickness, b_0 denotes the original substrate thickness. The mechanical stress balance assumed for the model is illustrated in (b).

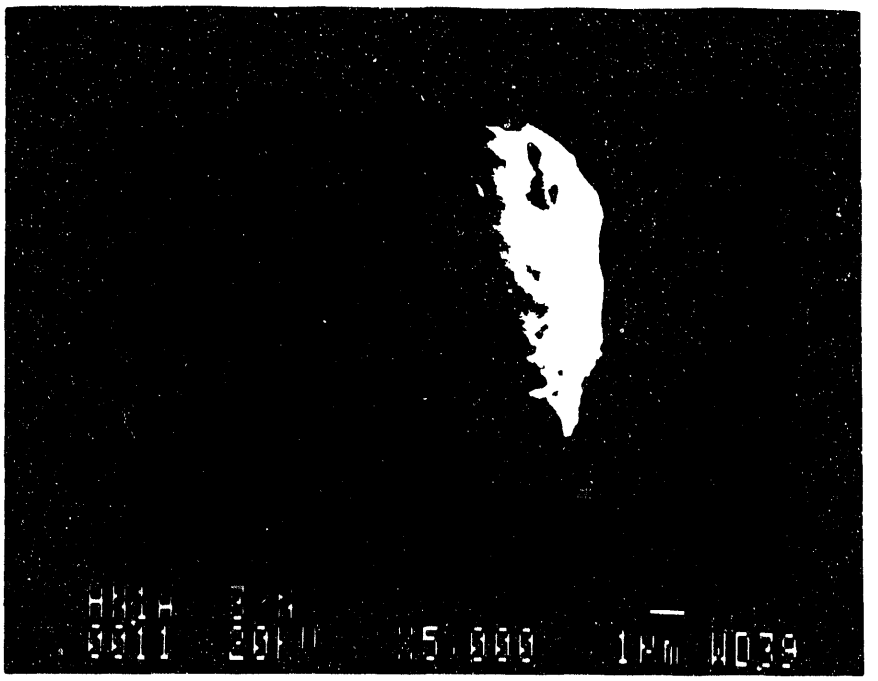

Figure 12. SEM micrograph of nano-indentation on NiO grown on Ni. Indentation has caused intergranular fracture in the oxide and severe plastic deformation of the Ni substrate.

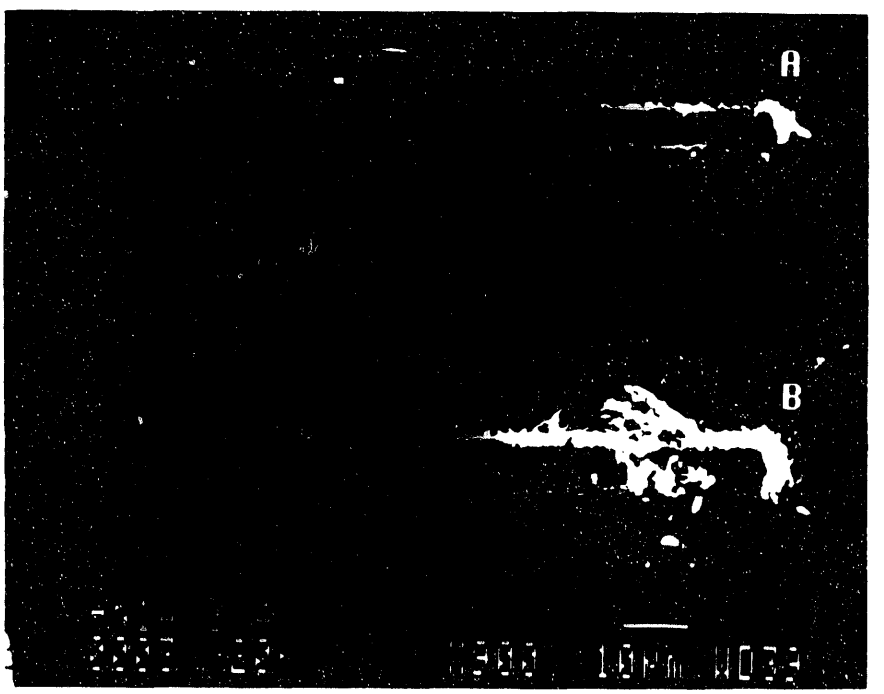

Figure 13. SEM micrograph of two scratch tracks on the NiO scale. The cracks within the indentor track, and perpendicular to the scratch path, are indicative of Mode I fracture. Localized oxide spallation has occurred on the track B.

END

DATE FILMED

12/29/92